IOP Conf. Series: Materials Science and Engineering **342** (2018) 012085 doi:10.1088/1757-899X/342/1/012085

Unsteady free convection flow past a semi-infinite vertical plate with constant heat flux in water based nanofluids

Marneni Narahari

Fundamental and Applied Sciences Department, Universiti Teknologi PETRONAS, 32610 Seri Iskandar, Malaysia

E-mail: marneni@utp.edu.my

Abstract. The unsteady free convective flow of nanofluids past a semi-infinite vertical plate with uniform heat flux has been investigated numerically. An implicit finite difference technique of Crank-Nicolson scheme has been employed to solve the governing partial differential equations. Five different types of water based nanofluids containing Cu, Ag, Al_2O_3, CuO and TiO_2 nanoparticles are considered to study the fluid flow characteristics with various time and solid volume fraction parameters. It is found that the local as well as the average Nusselt number for nanofluids is higher than the pure fluid (water). The local skin-friction is higher for pure fluid as compared to the nanofluids. The present numerical results obtained for local Nusselt number are validated with the previously published correlation results for a limiting case and it is found that the results are in good agreement.

1. Introduction

Nanofluids have received great attention lately due to its practical applications in many engineering and industrial processes. In 1995, Choi pioneered the concept of suspending ultra-fine particles in a base fluid and name it as nanofluid [1]. The promising outcome was obtained where the nanofluids exhibit higher thermal conductivity properties than pure fluid such as water, oil and ethylene glycol. According to Choi et al. [2], the thermal conductivity of nanofluid that consists of nanoparticles with total volume fraction less than 1% is approximately 2 times greater than pure fluid. Due to its enhanced thermal conductivity properties, nanofluids have wide applications especially in convective heat transfer which plays an important role in engineering processes such as the cooling system of electronic components, advanced nuclear system, solar collector, thermal insulation systems, food processes etc.

Convective heat transfer using nanofluid is an area that receives most scientific attention in the heat transfer research community. Most of the studies on convective heat transfer considered the steady state flow. Khan and Aziz [3] studied the steady free convective flow past a vertical plate with uniform surface heat flux in nanofluids. They highlighted that the reduced Nusselt number increased with the increase of Prandtl number, but decreased with the increase of Brownian motion, thermophoresis and the buoyancy ratio parameters. Chamkha and Rashad [4] investigated the steady state free convection flow past a permeable vertical cone embedded in a nanofluid filled porous medium under the uniform lateral heat and mass fluxes. It was concluded that an increase in the Lewis number increased both local Nusselt and Sherwood numbers. Tham et al. [5] investigated the steady mixed convection flow over a horizontal circular cylinder with constant heat flux in a porous medium filled by a nanofluid. They observed that the Brownian motion and buoyancy ratio parameters affected the fluid flow and heat transfer profiles.

Noghrehabadi et al. [6] numerically analyzed the natural convection flow of nanofluid over a vertical plate embedded in a Darcy porous medium subjected to surface heat and nanoparticle fluxes. They found that both reduced Nusselt and Sherwood numbers increased with the increase of Lewis number. Sheikholeslami et al. [7] presented the free convection flow of nanofluid in an enclosure with magnetic field. The control volume based finite element method was used to solve the governing equations and they found that the increase of Hartmann number reduced the rate of heat transfer while the augmentation of aspect ratio, nanoparticle volume fraction and Rayleigh number enhanced the rate of heat transfer. Jalilpour et al. [8] performed an investigation on the MHD stagnation-point nanofluid flow over a heated porous stretching surface with suction or blowing conditions and surface heat flux. The governing equations were solved through homotopy perturbation method (HPM). They concluded that an increase in the magnetic and thermophoresis parameters as well as Lewis number decreased the magnitude of the reduced Nusselt number. Reddy [9] performed an analysis of the natural convection flow of nanofluids over a vertical plate with uniform heat flux in the presence of thermal radiation. Similarity solutions were obtained using the fourth order Runge-Kutta method together with shooting technique and concluded that an increase in Prandtl number and radiation parameter increased the reduced Nusselt number. The natural convection flow of nanofluid past an inclined wavy surface with heat flux in a porous medium was analyzed by Srinivasacharya and Kumar [10] using the successive linearization method. They concluded that the local nanoparticle mass transfer coefficient increased and the local heat transfer coefficient decreased by increasing thermophoresis parameter. Trimbitas et al. [11] carried out an investigation on the steady mixed convection flow past a vertical semi-infinite flat plate in nanofluids. The governing equations were transformed to a system of coupled nonlinear ordinary differential equations using an appropriate similarity transformation and then solved numerically. They concluded that adding the nanoparticles into the based fluid (water) enhanced the skin-friction and heat transfer coefficient. All the above mentioned studies are confined to only convective heat transfer of steady state nanofluid flows.

The main purpose of the present paper is to investigate the unsteady free convective flow of water based nanofluid past a semi-infinite vertical plate with constant heat flux by using implicit finite difference technique of Crank-Nicolson scheme. This study is motivated by the need to explore the thermal performance of nanofluids in an unsteady state flow. A total of five different types of nanofluids, namely, Cu-water, Ag-water, CuO-water, TiO_2-water and Al_2O_3-water are taken into consideration. The influences of time and solid volume fraction on the fluid flow and heat transfer characteristics are discussed through graphs.

2. Mathematical analysis

Consider the unsteady two-dimensional free convective flow and heat transfer of a nanofluid past a semi-infinite vertical plate. The x'- axis is taken along the plate in the upward direction and the y'- axis is taken perpendicular to the plate into the fluid. Initially, the plate and the fluid are at the same temperature T'_∞. At time $t' > 0$, the surface of the plate is subject to a constant heat flux q'_w. The governing boundary layer equations of mass, momentum and energy for the free convective flow of nanofluid under the Boussinesq's approximation are as follows:

$$\frac{\partial u'}{\partial x'} + \frac{\partial v'}{\partial y'} = 0 \tag{1}$$

$$\rho_{nf}\left(\frac{\partial u'}{\partial t'} + u'\frac{\partial u'}{\partial x'} + v'\frac{\partial u'}{\partial y'}\right) = \mu_{nf}\frac{\partial^2 u'}{\partial y'^2} + g(\rho\beta)_{nf}(T' - T'_\infty) \tag{2}$$

$$(\rho C_P)_{nf}\left(\frac{\partial T'}{\partial t'} + u'\frac{\partial T'}{\partial x'} + v'\frac{\partial T'}{\partial y'}\right) = k_{nf}\frac{\partial^2 T'}{\partial y'^2} \tag{3}$$

The appropriate initial and boundary conditions are:

$$\left.\begin{array}{ll} t' \le 0: & u' = 0,\ v' = 0,\ T' = T'_\infty \quad \text{for all} \quad x', y' \\ t' > 0: & \begin{cases} u' = 0, v' = 0,\ \dfrac{\partial T'}{\partial y'} = -\dfrac{q'_w}{k_{nf}} & \text{at} \quad y' = 0 \\ u' = 0, v' = 0,\ T' = T'_\infty & \text{at} \quad x' = 0 \\ u' \to 0, v' \to 0,\ T' \to T'_\infty & \text{as} \quad y' \to \infty \end{cases} \end{array}\right\} \tag{4}$$

Where u' and v' are the velocity components in the x' and y' directions, respectively, T' is temperature of the fluid near the plate, T'_∞ is the temperature of the fluid far away from the plate, t' is the time, g is the acceleration due to gravity. μ_{nf} is the dynamic viscosity of the nanofluid, β_{nf} is the thermal expansion coefficient of the nanofluid, ρ_{nf} is the density of the nanofluid, k_{nf} is the thermal conductivity of the nanofluid, q'_w is the constant heat flux and $(C_p)_{nf}$ is the specific heat of the nanofluid which are given by:

$$\left.\begin{array}{l} \rho_{nf} = (1-\phi)\rho_f + \phi\rho_s \\ \mu_{nf} = \dfrac{\mu_f}{(1-\phi)^{2.5}} \\ (\rho\beta)_{nf} = (1-\phi)(\rho\beta)_f + \phi(\rho\beta)_s \\ (\rho C_P)_{nf} = (1-\phi)(\rho C_P)_f + \phi(\rho C_P)_s \\ k_{nf} = k_f \left[\dfrac{k_s + 2k_f - 2\phi(k_f - k_s)}{k_s + 2k_f + \phi(k_f - k_s)} \right] \end{array}\right\} \tag{5}$$

where ϕ is the solid volume fraction of the nanoparticles, ρ_f is the density of the base fluid, ρ_s is the density of the nanoparticles, μ_f is the viscosity of the base fluid, $(C_P)_f$ is the specific heat of the base fluid and $(C_P)_s$ is the specific heat of the nanoparticles. k_f is the thermal conductivity of the base fluid and k_s is the thermal conductivity of the nanoparticles.

The local as well as the average skin-friction and Nusselt number can be computed as follows:

$$\tau_{x'} = \mu_{nf}\left(\frac{\partial u'}{\partial y'}\right)_{y'=0} \tag{6}$$

$$Nu_{x'} = \frac{q'_w x'}{k_f (T' - T'_\infty)_{y'=0}}, \text{ where } q'_w = -k_{nf}\left(\frac{\partial T'}{\partial y'}\right)_{y'=0} \tag{7}$$

$$\tau_L = \frac{1}{L}\int_0^L \mu_{nf}\left(\frac{\partial u'}{\partial y'}\right)_{y'=0} dx' \tag{8}$$

$$Nu_L = \int_0^L \frac{q'_w}{k_f (T' - T'_\infty)_{y'=0}} dx' \tag{9}$$

Where $\tau_{x'}$ is the local skin-friction, $Nu_{x'}$ is the local Nusselt number, τ_L is the average skin-friction and Nu_L is the average Nusselt number.

On introducing the following non-dimensional quantities:

$$\left.\begin{aligned} &x=\frac{x'}{L},\ y=\frac{y'}{L}Gr^{1/4},\ t=\frac{t'\nu_f}{L^2}Gr^{1/2},\ u=\frac{u'L}{\nu_f}Gr^{-1/2},\ v=\frac{v'L}{\nu_f}Gr^{-1/4},\\ &\theta=\frac{T'-T'_\infty}{T^*},\ Gr=\frac{g\beta_f L^3T^*}{{\nu_f}^2},\mathrm{Pr}=\frac{\nu_f(\rho C_p)_f}{k_f}. \end{aligned}\right\} \tag{10}$$

Where $T^*=\frac{q'_wL}{k_f}Gr^{-1/4}$, x and y are the dimensionless coordinate axes, t is the dimensionless time, θ is the non-dimensional temperature, u and v are the non-dimensional velocity components in x and y directions, respectively, Gr and Pr are the Grashof and Prandtl numbers, respectively.

The non-dimensional governing equations are:

$$\frac{\partial u}{\partial x}+\frac{\partial v}{\partial y}=0 \tag{11}$$

$$\frac{\partial u}{\partial t}+u\frac{\partial u}{\partial x}+v\frac{\partial u}{\partial y}=a_1\frac{\partial^2 u}{\partial y^2}+a_2\theta \tag{12}$$

$$\left(\frac{\partial \theta}{\partial t}+u\frac{\partial \theta}{\partial x}+v\frac{\partial \theta}{\partial y}\right)=\frac{a_4}{\mathrm{Pr}\,a_3}\frac{\partial^2\theta}{\partial y^2} \tag{13}$$

The initial and boundary conditions are:

$$\left.\begin{array}{lll} t\le 0: & u=0,\ v=0,\ \theta=0 & \text{for all} \quad x,y\ge 0\\ t>0: & \left\{\begin{array}{lll} u=0,v=0,\ \frac{k_{nf}}{k_f}\frac{\partial\theta}{\partial y}=-1 & \text{at} & y=0\\ u=0,v=0,\ \theta=0 & \text{at} & x=0\\ u\to 0,v\to 0,\ \theta\to 0 & \text{as} & y\to\infty \end{array}\right. \end{array}\right\} \tag{14}$$

Where,

$$a_1=\frac{1}{(1-\phi)^{2.5}}\left[1/\{1-\phi+\phi(\rho_s/\rho_f)\}\right],\ a_2=\frac{1-\phi+\phi[(\rho\beta)_s/(\rho\beta)_f]}{1-\phi+\phi[\rho_s/\rho_f]},$$

$$a_3=1-\phi+\phi[(\rho C_P)_s/(\rho C_P)_f],\ a_4=\frac{k_{nf}}{k_f}=\left[\frac{k_s+2k_f-2\phi(k_f-k_s)}{k_s+2k_f+\phi(k_f-k_s)}\right].$$

Using the non-dimensional quantities specified in (10), the local as well as the average skin-friction and Nusselt number are as follows:

$$\tau_x/Gr^{3/4}=\frac{\tau_{x'}L^2}{\rho_f{\nu_f}^2}=\frac{1}{(1-\phi)^{2.5}}\left(\frac{\partial u}{\partial y}\right)_{y=0} \tag{15}$$

$$Nu_x/Gr^{1/4}=-a_4x\left[\left(\frac{\partial\theta}{\partial y}\right)_{y=0}\Big/(\theta)_{y=0}\right] \tag{16}$$

$$\tau/Gr^{3/4}=\frac{\tau_LL^2}{\rho_f{\nu_f}^2}=\frac{1}{(1-\phi)^{2.5}}\int_0^1\left(\frac{\partial u}{\partial y}\right)_{y=0}dx \tag{17}$$

$$Nu/Gr^{1/4} = -a_4 \int_0^1 \left[\left(\frac{\partial \theta}{\partial y} \right)_{y=0} \Big/ (\theta)_{y=0} \right] dx \tag{18}$$

3. Numerical technique

In order to solve the unsteady, non-linear coupled partial differential equations (11) to (13) under the conditions (14), an implicit finite difference scheme of Crank-Nicolson type has been employed. The finite difference equations corresponding to equations (11) to (13) are as follows:

$$\frac{u_{i,j-1}^{k+1} - u_{i-1,j-1}^{k+1} + u_{i,j-1}^{k} - u_{i-1,j-1}^{k} + u_{i,j}^{k+1} - u_{i-1,j}^{k+1} + u_{i,j}^{k} - u_{i-1,j}^{k}}{4\Delta x} + \frac{v_{i,j}^{k+1} - v_{i,j-1}^{k+1} + v_{i,j}^{k} - v_{i,j-1}^{k}}{2\Delta y} = 0 \tag{19}$$

$$\begin{aligned} &\frac{u_{i,j}^{k+1} - u_{i,j}^{k}}{\Delta t} + u_{i,j}^{k} \frac{\left[u_{i,j}^{k+1} - u_{i-1,j}^{k+1} + u_{i,j}^{k} - u_{i-1,j}^{k} \right]}{2\Delta x} + v_{i,j}^{k} \frac{\left[u_{i,j+1}^{k+1} - u_{i,j-1}^{k+1} + u_{i,j+1}^{k} - u_{i,j-1}^{k} \right]}{4\Delta y} \\ &= a_1 \frac{\left[u_{i,j-1}^{k+1} - 2u_{i,j}^{k+1} + u_{i,j+1}^{k+1} + u_{i,j-1}^{k} - 2u_{i,j}^{k} + u_{i,j+1}^{k} \right]}{2(\Delta y)^2} + a_2 \frac{\left[\theta_{i,j}^{k+1} + \theta_{i,j}^{k} \right]}{2} \end{aligned} \tag{20}$$

$$\begin{aligned} &\frac{\theta_{i,j}^{k+1} - \theta_{i,j}^{k}}{\Delta t} + u_{i,j}^{k} \frac{\left[\theta_{i,j}^{k+1} - \theta_{i-1,j}^{k+1} + \theta_{i,j}^{k} - \theta_{i-1,j}^{k} \right]}{2\Delta x} + v_{i,j}^{k} \frac{\left[\theta_{i,j+1}^{k+1} - \theta_{i,j-1}^{k+1} + \theta_{i,j+1}^{k} - \theta_{i,j-1}^{k} \right]}{4\Delta y} \\ &= \frac{a_4}{\Pr a_3} \frac{\left[\theta_{i,j-1}^{k+1} - 2\theta_{i,j}^{k+1} + \theta_{i,j+1}^{k+1} + \theta_{i,j-1}^{k} - 2\theta_{i,j}^{k} + \theta_{i,j+1}^{k} \right]}{2(\Delta y)^2} \end{aligned} \tag{21}$$

The finite-difference form of the thermal boundary condition at $y = 0$ can be written as

$$a_4 \left[\frac{\theta_{i,1}^{k+1} - \theta_{i,-1}^{k+1} + \theta_{i,1}^{k} - \theta_{i,-1}^{k}}{4\Delta y} \right] = -1 \tag{22}$$

At $y = 0$ (i.e., $j = 0$), the finite-difference equation (21) for energy equation becomes

$$\begin{aligned} &\frac{\theta_{i,0}^{k+1} - \theta_{i,0}^{k}}{\Delta t} + u_{i,0}^{k} \frac{\left[\theta_{i,0}^{k+1} - \theta_{i-1,0}^{k+1} + \theta_{i,0}^{k} - \theta_{i-1,0}^{k} \right]}{2\Delta x} \\ &= \frac{a_4}{\Pr a_3} \frac{\left[\theta_{i,-1}^{k+1} - 2\theta_{i,0}^{k+1} + \theta_{i,1}^{k+1} + \theta_{i,-1}^{k} - 2\theta_{i,0}^{k} + \theta_{i,1}^{k} \right]}{2(\Delta y)^2} \end{aligned} \tag{23}$$

After eliminating $\theta_{i,-1}^{k+1} + \theta_{i,-1}^{k}$ from Eq. (23) using Eq. (22), the finite-difference equation for the energy equation (13) at the boundary reduces to the form

$$\begin{aligned} &\frac{\theta_{i,0}^{k+1} - \theta_{i,0}^{k}}{\Delta t} + u_{i,0}^{k} \frac{\left[\theta_{i,0}^{k+1} - \theta_{i-1,0}^{k+1} + \theta_{i,0}^{k} - \theta_{i-1,0}^{k} \right]}{2\Delta x} \\ &= \frac{a_4}{\Pr a_3} \frac{\left[-\theta_{i,0}^{k+1} + \theta_{i,1}^{k+1} - \theta_{i,0}^{k} + \theta_{i,1}^{k} + 2(\Delta y / a_4) \right]}{(\Delta y)^2} \end{aligned} \tag{24}$$

To solve the above equations, the region of integration is considered as a rectangle with sides $x_{\max}\,(=1)$ and $y_{\max}\,(=7)$, where $y_{\max}$ corresponds to $y \to \infty$ which lies very well outside the momentum and energy boundary layers. The maximum value of *y* is chosen as 7 after some preliminary investigations so that the last two of the boundary conditions in (14) are satisfied. Here, the subscript *i*-designates the grid point along the *x*-direction, *j* along the *y*-direction and the superscript *k* along the *t*-direction. An appropriate mesh size considered for the calculation is $\Delta x = 0.01$, $\Delta y = 0.05$, and time step $\Delta t = 0.01$.

During any one time step, coefficients $u_{i,j}^{n}$ and $v_{i,j}^{n}$ appearing in the difference equations are treated as constants. The values of *u*, *v* and θ are known at all grid points at *t* = 0 from the initial conditions. The computations of *u*, *v* and θ at time level $(k+1)$ using the known values at previous time level (*k*) are calculated as follows: The finite difference equation (21) at every internal nodal point on a particular *i*-level constitute a tri-diagonal system of equations. Such a system of equations is solved by Thomas algorithm as described in Carnahan et al. [12]. The values of θ are calculated from equation (21). Using the values of θ at $(k+1)^{th}$ time level in the equation (20), the values of *u* at $(k+1)^{th}$ time level are found in a similar manner. Thus the values of θ and *u* are known on a particular *i*-level. The values of *v* are calculated explicitly using the equation (19) at every nodal point on a particular *i*-level at $(k+1)^{th}$ time level. This process is repeated for various *i*-levels. Thus the values of θ, *u* and *v* are known at all grid points in the rectangular region at $(k+1)^{th}$ time level.

4. Results and discussion

The unsteady free convection flow past a semi-infinite vertical plate with constant heat flux in water based nanofluids such as Cu-water, Ag-water, CuO-water, TiO_2-water and Al_2O_3-water are investigated numerically by employing an implicit finite difference technique of Crank-Nicolson scheme. The thermo-physical properties of water and nanoparticles are shown in Table 1. The numerical results are illustrated graphically and discussed thoroughly in order to get an in depth study on the relationship between various factors. Table 2 illustrates the comparison of the current numerical results of steady state local Nusselt number with pure fluid correlation results of Chen et al. [13] when $\phi = 0$. It is observed that the comparison outcome is in good agreement and this justifies the accuracy of the present numerical technique.

Table 1. Thermo-physical properties of water and nanoparticles.

	ρ (Kg/m^3)	C_p (J/Kg.K)	k (W/m.K)	$\beta \times 10^5$ (K^{-1})
Water	997.1	4179	0.613	21
Ag	10500	235	429	1.89
Cu	8933	385	401	1.67
Al_2O_3	3970	765	40	0.85
CuO	6320	531.8	76.5	1.80
TiO_2	4250	686.2	8.9538	0.9

Table 2. Comparison of the local Nusselt numbers when $\phi = 0$ with the correlation results of Chen et al. [13] for regular fluids.

Pr	Local Nusselt Number	
	Chen et al. [13]	Present
1	0.5341	0.5344
7	0.8709	0.8704
10	0.9453	0.9447
15	1.0356	1.0348
20	1.1037	1.1027
50	1.3452	1.3437
100	1.5567	1.5547
500	2.1692	2.1655
1000	2.4976	2.4929

The effect of time on both velocity and temperature profiles of Al_2O_3-water nanofluid are depicted in Figures 1 and 2. It is noticed that both velocity and temperature profiles increase prominently with the increase of time until the fluid achieves steady state conditions at $t = 9.5$ when $\mathrm{Pr} = 6.2$ and $\phi = 0.04$. The prolonged time enables more heat to transfer from the plate to the fluid, causing an increase in the fluid temperature and buoyancy effect, and hence, the fluid velocity increases as well. Figure 1 shows that the velocity increases to a maximum value near the vertical plate, then it decays as the distance from the vertical plate increases till it satisfies the free stream condition. The maximum velocity increases significantly and formed further away from the plate with the increase of time. Figure 2 demonstrates that the temperature declines gradually to a free stream temperature as the distance from the vertical plate increases.

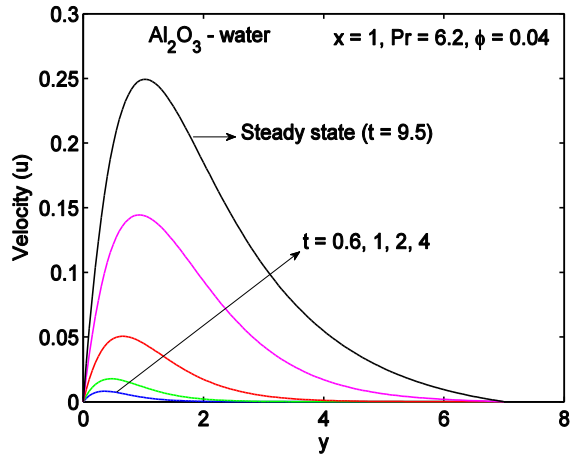

Figure 1. Velocity profiles at different t for Al_2O_3-water nanofluid.

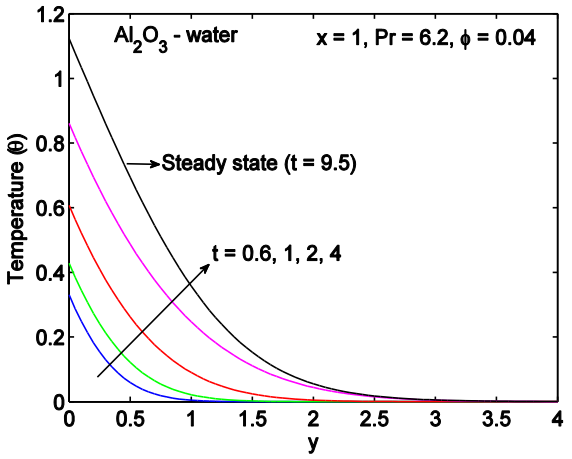

Figure 2. Temperature profiles at different t for Al_2O_3-water nanofluid.

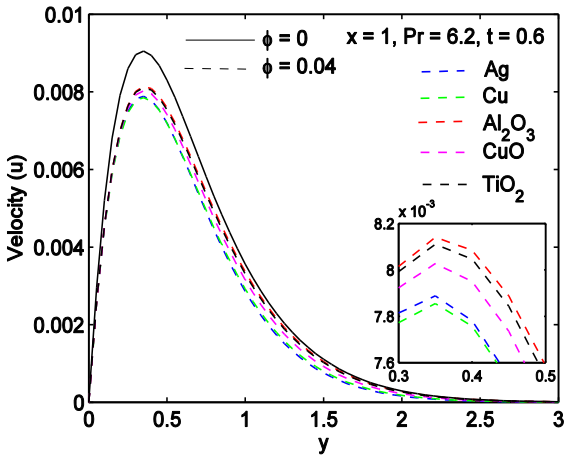

Figure 3. Velocity profiles of nanofluids at different ϕ.

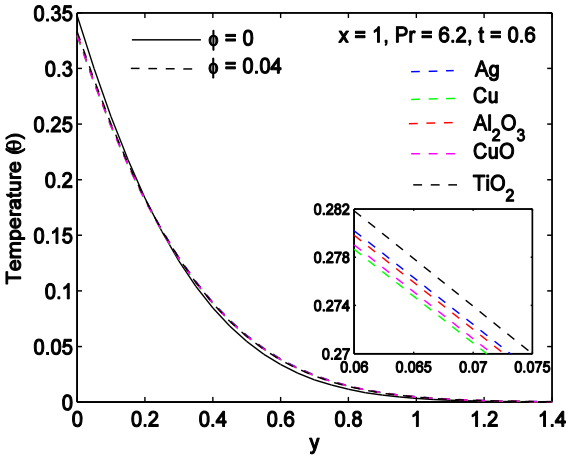

Figure 4. Temperature profiles of nanofluids at different ϕ.

The velocity and temperature profiles of pure fluid and nanofluids with the volume fraction of 0.04 are shown in Figures 3 and 4, respectively. The velocity rises rapidly to a peak value near the vertical plate, then it drops as the distance from the vertical plate increases until the free stream boundary condition is satisfied. The maximum velocity of the pure fluid and the nanofluids are formed in the vicinity of the plate and at the same distance from the vertical plate. The pure fluid exhibits higher velocity profile compared to nanofluids while Al_2O_3-water has the highest velocity profile among the nanofluids and Cu-water has the lowest. It is seen from Figure 4 that the temperature decays gradually to a free stream temperature as the distance from the vertical plate increases. The pure fluid has higher temperature

profile than nanofluids in close proximity to the vertical plate but the temperature profile of pure fluid is lower than that of nanofluids after a certain distance from the plate. Figure 4 also shows that nanofluids exhibit minor variations in temperature profiles. A further scrutiny reveals that TiO_2-water has the highest temperature profile while Cu-water has the lowest among the nanofluids. However, the trend changes after a certain distance from the vertical plate where Ag-water has the highest temperature profile whilst TiO_2-water has the lowest.

The local skin-friction and local Nusselt number variations for various nanofluids with the volume fraction of 0.04 and pure fluid are depicted in Figures 5 and 6, respectively. It is observed that the local skin-friction escalates drastically and reaches steady state near the leading edge. A prominent variation in the local skin-friction can be seen once the fluids achieve steady state along the vertical plate. Compared to nanofluids, the pure fluid has higher local skin-friction while Ag-water possesses slightly maximum and Cu-water possesses the minimum local skin-friction among the nanofluids. It is seen from Figure 6 that the local Nusselt number increases linearly with the distance along the vertical plate. Nanofluids have the higher local Nusselt number than pure fluid due to the addition of nanoparticles that enhances the fluid thermal conductivity. Meanwhile, Cu-water possesses the maximum and TiO_2-water possesses the minimum local Nusselt number among the nanofluids.

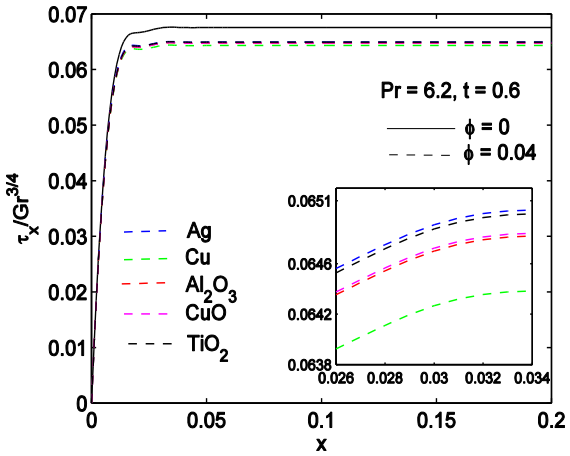

Figure 5. Local skin-friction variation for nanofluids at different ϕ.

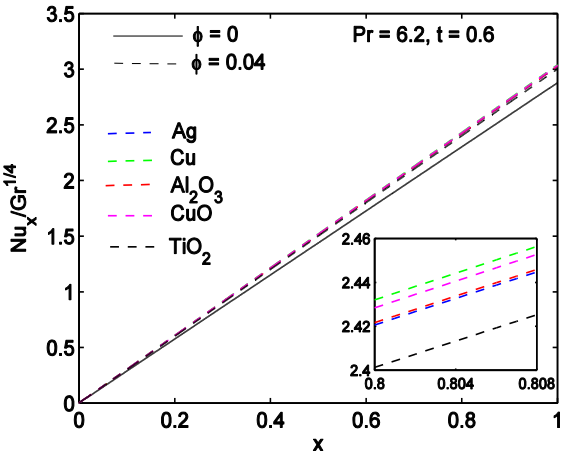

Figure 6. Local Nusselt number variation for nanofluids at different ϕ.

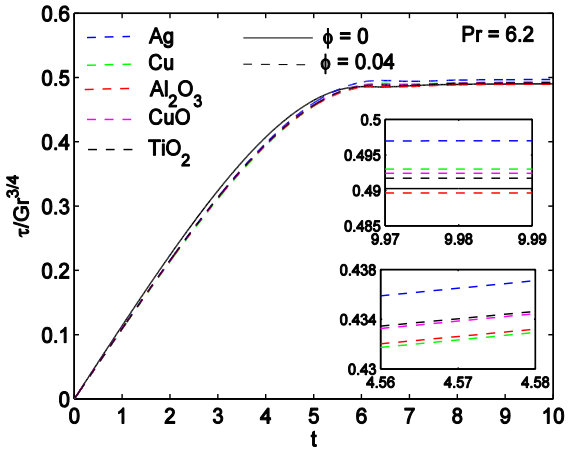

Figure 7. Average skin-friction variation for nanofluids at different ϕ.

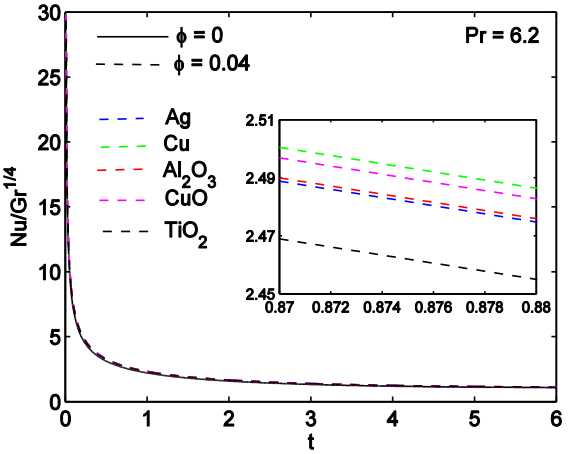

Figure 8. Average Nusselt number variation for nanofluids at different ϕ.

The average skin-friction and Nusselt number variations with time for nanofluids and pure fluid are illustrated in Figures 7 and 8, respectively. The average skin-friction increases as time progress until it reaches the steady state. Pure fluid exhibits higher average skin-friction compared to nanofluids during the transient state, thereafter the average skin-friction for pure fluid is lower than nanofluids instead. Among the nanofluids, Ag-water causes the most average skin-friction while Al_2O_3-water causes the least in the steady state. From Figure 8, it is observed that the average Nusselt number experiences a sudden drop at small values of time till it reaches steady state as time progresses. However, the nanofluids with volume fraction of 0.04 and pure fluid exhibit meagre variations of average Nusselt numbers. A close observation on the graph reveals that pure fluid has lower average Nusselt number compared to nanofluids while Cu-water has the maximum and TiO_2-water has the minimum average Nusselt number among the nanofluids.

5. Conclusions

In this paper, the unsteady free convection flow past a semi-infinite vertical plate with constant heat flux in water based nanofluids has been investigated numerically using an implicit finite difference technique of Crank-Nicolson type. The accuracy of the present numerical scheme is verified by comparing the local Nusselt number with the well-known pure fluid correlation results and the outcome is excellent. The flow characteristics with different time and solid volume fraction are discussed and the important conclusions are listed below:

1. An increase in time leads to increase in temperature and velocity profiles of nanofluid until they reach steady state profiles.
2. Al_2O_3-water nanofluid has the highest velocity profile while Cu-water nanofluid has the lowest among the nanofluids chosen.
3. TiO_2-water and Cu-water have the highest and lowest temperature profiles, respectively, near to the vertical plate. However, Ag-water has the highest temperature profile whilst TiO_2-water has the lowest after a certain distance from the plate.
4. The pure fluid causes higher local and average skin-frictions compared to the nanofluids.
5. The pure fluid has lower local and average Nusselt numbers compared to the nanofluids.
6. Ag-water nanofluid has the maximum and Cu-water nanofluid has the minimum local skin-friction.
7. Cu-water nanofluid has the maximum and TiO_2-water nanofluid has the minimum local Nusselt number.
8. Ag-water nanofluid has the maximum and Al_2O_3-water nanofluid has the minimum average skin-friction.
9. Cu-water nanofluid has the maximum and TiO_2-water nanofluid has the minimum average Nusselt number.

Acknowledgement

The author would like to thank Universiti Teknologi PETRONAS for the financial assistance provided by the research grant YUTP 0153AA-E28.

References

[1] Choi S U S and Eastman J 1995 Enhancing thermal conductivity of fluids with nanoparticles, The Proceedings of the 1995 ASME International Mechanical Engineering Congress and Exposition, San Francisco, USA, ASME, FED 231/MD66. 99-105.

[2] Choi S, Zhang Z, Yu W, Lockwood F and Grulke E 2001 Anomalously thermal conductivity enhancement in nanotube suspensions *Appl. Phys. Lett*. **79** 2252

[3] Khan W A and Aziz A 2011 Natural convection flow of a nanofluid over a vertical plate with uniform surface heat flux *Int. J. Therm. Sci*. **50** 1207

[4] Chamkha A J and Rashad A M 2012 Natural convection from a vertical permeable cone in a nanofluid saturated porous media for uniform heat and nanoparticles volume fraction fluxes *Int. J. Numer. Methods Heat Fluid Flow* **22** 1073

[5] Tham L, Nazar R and Pop I 2016 Mixed convection flow over a horizontal circular cylinder with constant heat flux embedded in a porous medium filled by a nanofluid: Buongiorno-Darcy model *Heat Mass Transf.* **52** 1983
[6] Noghrehabadi A, Behrseresht A and Ghalambaz M 2013 Natural convection of nanofluid over vertical plate embedded in porous medium: Prescribed surface heat flux *Appl. Math. Mech. – Engl. Ed.* **34** 669
[7] Sheikholeslami M, Gorji-Bandpy M, Ganji D D and Soleimani S 2014 Heat flux boundary condition for nanofluid filled enclosure in presence of magnetic field *J. Mol. Liq*. **193** 174
[8] Jalilpour B, Jafarmadar S, Ganji D D, Shotorban A B and Taghavifar H 2014 Heat generation/absorption on MHD stagnation flow of nanofluid towards a porous stretching sheet with prescribed surface heat flux *J. Mol. Liq*. **195** 194
[9] Reddy M G 2014 Influence of thermal radiation on natural convection boundary layer flow of a nanofluid past a vertical plate with uniform heat flux *International Journal of Heat and Technology* **32** 1
[10] Srinivasacharya D and Kumar P V 2015 Free convection of a nanofluid over an inclined wavy surface embedded in a porous medium with wall heat flux *Procedia Engineering* **127** 40
[11] Trimbitas R, Grosan T and Pop I 2015 Mixed convection boundary layer flow past vertical flat plate in nanofluid: case of prescribed wall heat flux *Appl. Math. Mech. -Engl. Ed*. **36** 1091
[12] Carnahan B, Luther H A and Wilkes J O 1969 Applied Numerical Methods, Jhon Wiley & Sons, New York
[13] Chen T S, Tien H C and Armaly B F 1986 Natural convection on horizontal, inclined, and vertical plates with variable surface temperature or heat flux *Int. J. Heat Mass Transf.* **19** 1465